Chapter 5

Enhanced Single-Phase Turbulent Tube-side Flows and Heat Transfer

SUMMARY: This section presents methods for predicting heat transfer and pressure drop for turbulent flows inside corrugated tubes, internally ribbed or finned tubes, and in tubes with twisted tape inserts. A brief review of prediction methods for turbulent flow heat transfer in plain tubes is also presented for the reader's convenience and the important issues of inlet configuration effects on heat transfer and pressure drop in the transition region between laminar and turbulent flows in plain tubes are addressed.

5.1 Introduction

This chapter covers turbulent flow and heat transfer inside plain and enhanced tubes. Only tubular enhancement geometries of particular industrial interest are discussed here. These geometries are corrugated tubes, internally finned or ribbed tubes, and tubes with twisted tape inserts. The commonly used prediction methods for heat transfer and pressure drop for plain tubes are first presented and then the mechanisms of heat transfer augmentation are discussed. Next, design methods for corrugated tubes, internally finned or ribbed tubes, and tubes with twisted tape inserts are presented. The reader is referred to other sources for more detailed reviews of the literature and experimental results, such as the book of Webb (1994).

Tubular enhancements made by Wolverine Tube Inc. include corrugated tubes and tubes with integral internal fins or ribs. Figure 5.1 shows a diagram of a single-start corrugated tube and Figure 5.2 depicts a photograph of a Wolverine Korodense corrugated tube. A corrugated tube is defined geometrically by the corrugation pitch, p, and the corrugation depth, e. The axial corrugation pitch is related to the internal diameter d_i, helix angle β relative to the axis of the tube and the number of starts n_s by the following geometrical equation:

$$p = \frac{\pi\, d_i}{n_s \tan\beta} \qquad [5.1.1]$$

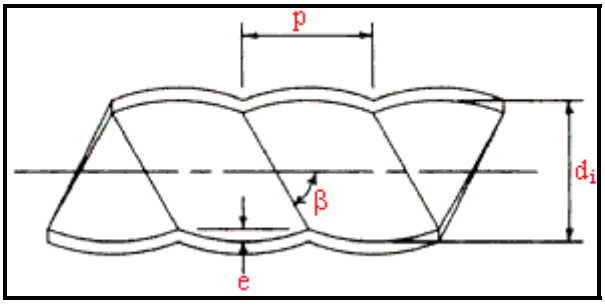

Figure 5.1. Diagram of corrugated tube.

Figure 5.2. Photograph of Wolverine Korodense tube.

The external diameter over the corrugations on the outside of the tube is equal to that of the plain ends of the tube. The internal diameter is taken as the external diameter less twice the tube wall thickness. The internal area ratio of a corrugated tube relative to a plain tube of the same diameter d_i is slightly larger than one.

Figure 5.3 depicts a schematic diagram for an internally finned or ribbed tube. As it is difficult to geometrically define a difference between a fin and a rib, these two names will be assumed to refer to the same geometry here. Helical internal *fins* or *ribs* (or also referred to as *ridges* in Wolverine Tube literature) are applied to the inside of low finned tubes such as Turbo-Chil and S/T Trufin and to enhanced boiling and condensing tubes, such as the various versions of Turbo-B and Turbo-C. The internal fin (or rib or ridge) geometry is defined by the fin height, the mean fin thickness, the apex angle of the fin, the helix angle of the fin and the axial pitch of one fin to the next. The helix angle is related to the axial fin pitch by applying the expression above using the number of fins in place of the number of starts. The internal area ratio relative to a plain tube of the same diameter d_i ranges from about 1.3 to 2.0. The internal fins can be of various cross-sectional shapes. Most industrial tubes have fins (or ribs or ridges) with a trapezoidal cross-sectional profile (wider at the base than at the tip of the fin and with rounded corners). Figure 5.4 shows a photograph of a Wolverine Turbo-Chil low finned tube with internal helical fins.

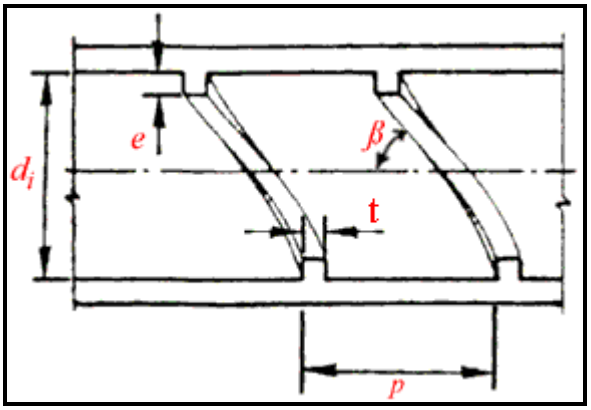

Figure 5.3. Diagram of internally finned or ribbed tube.

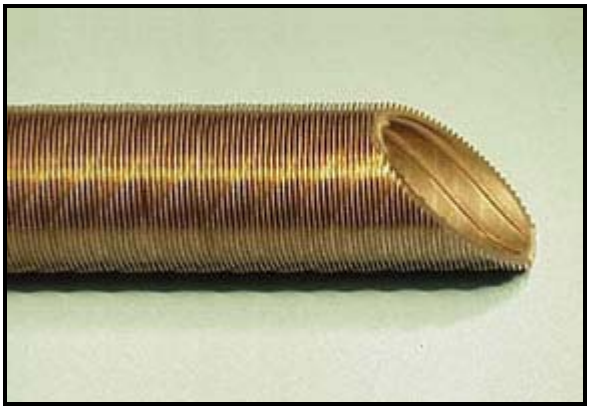

Figure 5.4. Photograph of Wolverine Turbo-Chil tube.

5.2 Turbulent and Transition Flows and Heat Transfer in Plain Tubes

Before discussing heat transfer enhancement of turbulent, single-phase flows inside tubes, a summary of turbulent and transitions flows inside plain tubes and the effects of the tube inlet configuration on heat transfer and transition thresholds are presented below.

The most commonly used correlation for predicting fully developed turbulent flow heat transfer coefficients inside smooth, round tubes is what is known as the Dittus-Boelter (1930) equation:

$$Nu = \frac{\alpha_{pt}\, d_i}{k} = 0.023\, Re^{0.8}\, Pr^n \qquad [5.2.1]$$

where the Nusselt number Nu is based on the tube diameter d_i and α_{pt} is the convective heat transfer coefficient for a plain tube. The tubular Reynolds number Re is defined as:

$$\mathrm{Re} = \frac{\dot{m}\, d_i}{\mu} \qquad [5.2.2]$$

The mass velocity $\dot{m}$ is in kg/m^{2}s and is obtained by dividing the mass flow rate in kg/s by the cross-sectional area of the tube in m^2. The Prandtl number Pr is obtained from the physical properties of the fluid and is defined as:

$$\mathrm{Pr} = \frac{c_p \mu}{k} \qquad [5.2.3]$$

The exponent on the Prandtl number for cooling a fluid is n = 0.3 (for $T_{wall} < T_{bulk}$) while for heating a fluid is n = 0.4 (for $T_{wall} > T_{bulk}$), where T_{wall} is the inside tube wall temperature and T_{bulk} is the mean fluid temperature. In the above expressions, the fluid properties are as follows: c_p is the specific heat at constant pressure, k is the thermal conductivity, and μ is the dynamic viscosity. This correlation is generally accurate to about ±25% as has been confirmed experimentally for the following range of conditions: $0.7 \le \mathrm{Pr} \le 160$, $\mathrm{Re} \ge 10^4$ and $L/d_i \ge 10$ where L is the length from the inlet of the tube. This expression may be used for moderate temperature differences with fluid properties evaluated at the bulk fluid temperature.

Another widely used method from the same time period is that of Sieder and Tate (1936), who recommended the following expression for applications with large property variations from the bulk flow to the wall temperature:

$$\mathrm{Nu} = \frac{\alpha_{pt}\, d_i}{k} = 0.027\, \mathrm{Re}^{0.8}\, \mathrm{Pr}^{1/3} \left(\frac{\mu_{bulk}}{\mu_{wall}} \right)^{0.14} \qquad [5.2.4]$$

for $0.7 < \mathrm{Pr} < 16000$, $\mathrm{Re} > 10000$ and $L/D > 10$.

For more accurate calculations in fully developed turbulent flow (to within about ±10%), it is recommended to use the Petukhov (1970) heat transfer correlation that is valid for $0.5 < \mathrm{Pr} < 2000$ and $10^4 < \mathrm{Re} < 5 \times 10^6$:

$$\mathrm{Nu} = \frac{\alpha_{pt}\, d_i}{k} = \frac{(f/2)\,\mathrm{Re}\,\mathrm{Pr}}{1.07 + 12.7(f/2)^{1/2}\left(\mathrm{Pr}^{2/3} - 1\right)} \left(\frac{\mu_{bulk}}{\mu_{wall}} \right)^{0.14} \qquad [5.2.5]$$

where the friction factor f can be obtained from the Moody diagram or from Petukhov's friction factor correlation for smooth tubes valid for $3000 < \mathrm{Re} < 5 \times 10^6$:

$$f = \left(1.58 \ln \mathrm{Re} - 3.28\right)^{-2} \qquad [5.2.6]$$

The property ratio $(\mu_{bulk}/\mu_{wall})^{0.14}$ corrects for property variations for liquid flows being heated or cooled, where μ_{bulk} is that at the mean fluid temperature T_{bulk} and μ_{wall} is that at the wall temperature T_{wall}. No property correction is used for a gas being cooled while the viscosity ratio term is replaced by a

temperature ratio $[(T_{bulk}+273)/(T_{wall}+273)]^{0.25}$ for a gas being heated. Similar corrections should be applied to the friction factor expression above but with the exponent as negative value, where -0.25 is the most often quoted but some texts also recommend a value of -0.14. The other properties are evaluated at the bulk temperature. The pressure drop in a tube of length L is given by the expression:

$$\Delta p = \frac{2 f \dot{m}^2 L}{\rho d_i} \qquad [5.2.7]$$

Another heat transfer correlation commonly used is that of Gnielinski (1976), which extends the Petukhov correlation down into the transition regime:

$$Nu = \frac{\alpha_{pt}\, d_i}{k} = \frac{(f/2)(Re-1000)Pr}{1+12.7(f/2)^{1/2}(Pr^{2/3}-1)}\left(\frac{\mu_{bulk}}{\mu_{wall}}\right)^{0.14} \qquad [5.2.8]$$

where the friction factor f is obtained from Petukhov's friction factor correlation above or from the Moody diagram. It is accurate to about 10% for the following conditions: $0.5 < Pr < 2000$ and $3000 < Re < 5 \times 10^6$. Flow is normally considered to be fully developed starting from about 10 to 60 tube diameters from the entrance (see additional discussion below).

Ghajar and coworkers in a series of papers have investigated the ***transition region*** between laminar and turbulent flow in plain tubes experimentally and also proposed some prediction methods for this regime to bridge between laminar methods and turbulent methods, applicable to forced and mixed convection in the entrance and fully developed regions for three types of inlet configurations: re-entrant (tube extends beyond tubesheet face into head of distributor, square-edged (tube end is flush with tubesheet face) and bell-mouth (a tapered entrance of tube from tubesheet face). Ghajar, Tam and Tam (2004) give a summary of all their heat transfer work and propose an artificial neural network approach for modelling their heat transfer data. Earlier, Ghajar and Tam (1994) proposed an easier to implement method that also captured all the trends with nearly the same accuracy, which is presented below. The local heat transfer coefficient in transition flow is obtained from the transition Nusselt number, Nu_{trans}, which is calculated as follows at a distance z from the entrance:

$$Nu_{trans} = Nu_{lam} + \left\{\exp[(a-Re)/b] + Nu_{turb}^{c}\right\}^{c} \qquad [5.2.9]$$

where Nu_{lam} is the laminar flow Nusselt number for entrance region laminar flows with natural convection effects:

$$Nu_{lam} = 1.24\left[\left(\frac{Re\, Pr\, d_i}{z}\right) + 0.025(Gr\, Pr)^{0.75}\right]^{1/3}\left(\frac{\mu_{bulk}}{\mu_{wall}}\right)^{0.14} \qquad [5.2.10]$$

and Nu_{turb} is the turbulent flow Nusselt number with developing flow effects:

$$Nu_{turb} = 0.023\, Re^{0.8}\, Pr^{0.385}\left(\frac{z}{d_i}\right)^{-0.0054}\left(\frac{\mu_{bulk}}{\mu_{wall}}\right)^{0.14} \qquad [5.2.11]$$

The Nusselt, Reynolds and Prandtl numbers have their traditional definitions. The Grashof number Gr is defined as:

$$Gr = g\beta_{th}\rho^2 d_i^3 \left(T_{wall} - T_{bulk}\right)/\mu^2 \qquad [5.2.12]$$

In this expression the inner tube wall temperature is T_{wall}, the bulk fluid temperature is T_{bulk}, β_{th} is the coefficient of thermal expansion of the fluid at the bulk temperature, g is the acceleration due to gravity (9.81 m/s^2) and z is the distance from the entrance of the tube whose diameter is d_i. The physical properties (k, μ, ρ, c_p) appearing in the dimensionless numbers (Nu, Re, Pr and Gr) are all evaluated at the bulk fluid temperature (T_{bulk}). The values of the empirical constants a, b and c in [5.2.9] depend on the inlet configuration and are given in Table 5.1. The viscosity ratio accounts for the temperature effect on the process. The range of application of the heat transfer method based on their database of 1290 points (441 points for re-entrant inlet, 416 for square-edged inlet and 433 points for bell-mouth inlet) is as follows:

Re-entrant: $3 \le z/d_i \le 192$, $1700 \le Re \le 9100$, $5 \le Pr \le 51$, $4000 \le Gr \le 210000$, $1.2 \le \mu_{bulk}/\mu_{wall} \le 2.2$.

Square-edged: $3 \le z/d_i \le 192$, $1600 \le Re \le 10700$, $5 \le Pr \le 55$, $4000 \le Gr \le 250000$, $1.2 \le \mu_{bulk}/\mu_{wall} \le 2.6$.

Bell-mouth: $3 \le z/d_i \le 192$, $3300 \le Re \le 11100$, $13 \le Pr \le 77$, $6000 \le Gr \le 110000$, $1.2 \le \mu_{bulk}/\mu_{wall} \le 3.1$.

Table 5.1. Constants for transition heat transfer and pressure drop correlations.

Inlet geometry	a	B	c	A	B	C	m_1	m_2	m_3	m_4
Re-entrant	1766	276	-0.955	5840	-0.0145	-6.23	-1.10	0.460	-0.133	4.10
Square-edged	2617	207	-0.950	4230	-0.1600	-6.57	-1.13	0.396	-0.160	5.10
Bell-mouth	6628	237	-0.980	5340	-0.0990	-6.32	-2.58	0.420	-0.410	2.46

These methods capture about 70% of their data within an error band of ±10% and 97% of their data within ±20%, which is remarkable for transition flows. The individual expressions above for Nu_{lam} and Nu_{turb} can be used alone for developing flows in those respective regimes. The lower and upper limits of the transition regime occur at the following conditions according to Ghajar and Tam (1995):

Re-entrant:
$$Re(\text{lower}) = 2157 - 0.65\left[192 - (z/d_i)\right] \qquad [5.2.13a]$$
$$Re(\text{upper}) = 8475 - 9.28\left[192 - (z/d_i)\right] \qquad [5.2.13b]$$

Square-edged:
$$Re(\text{lower}) = 2524 - 0.82\left[192 - (z/d_i)\right] \qquad [5.2.14a]$$
$$Re(\text{upper}) = 8791 - 7.69\left[192 - (z/d_i)\right] \qquad [5.2.14b]$$

Bell-mouth:
$$Re(\text{lower}) = 3787 - 1.80\left[192 - (z/d_i)\right] \qquad [5.2.15a]$$
$$Re(\text{upper}) = 10481 - 5.47\left[192 - (z/d_i)\right] \qquad [5.2.15b]$$

The above equations indicate that the re-entrant inlet configuration causes the earliest transition from laminar flow into the transition regime (at about 2000) while the bell-mouth entrance retards this regime change (at about 3500). The square-edged entrance falls in between (at about 2400), which is close to the often quoted value of 2300 in most textbooks. Figure 5.5 clearly shows the influence of inlet configuration on the beginning and end of the heat transfer transition region. This figure plots the local

average peripheral heat transfer coefficients in terms of the Colburn j factor (St $Pr^{0.67}$) versus local Reynolds number for all flow regimes at the length-to-diameter ratio of 192, and St is the Stanton number (Nu/(Re Pr)). The filled symbols represent the start and end of the heat transfer transition region for each inlet configuration. Note the large influence of natural convection superimposed on the forced convective laminar flow heat transfer process (Nu = 4.364 for a fully developed laminar flow with a uniform heat flux boundary condition without buoyancy effects), yielding a mixed convection value of about Nu = 14.5. Expression [5.2.10] includes this buoyancy effect through the Grashof number.

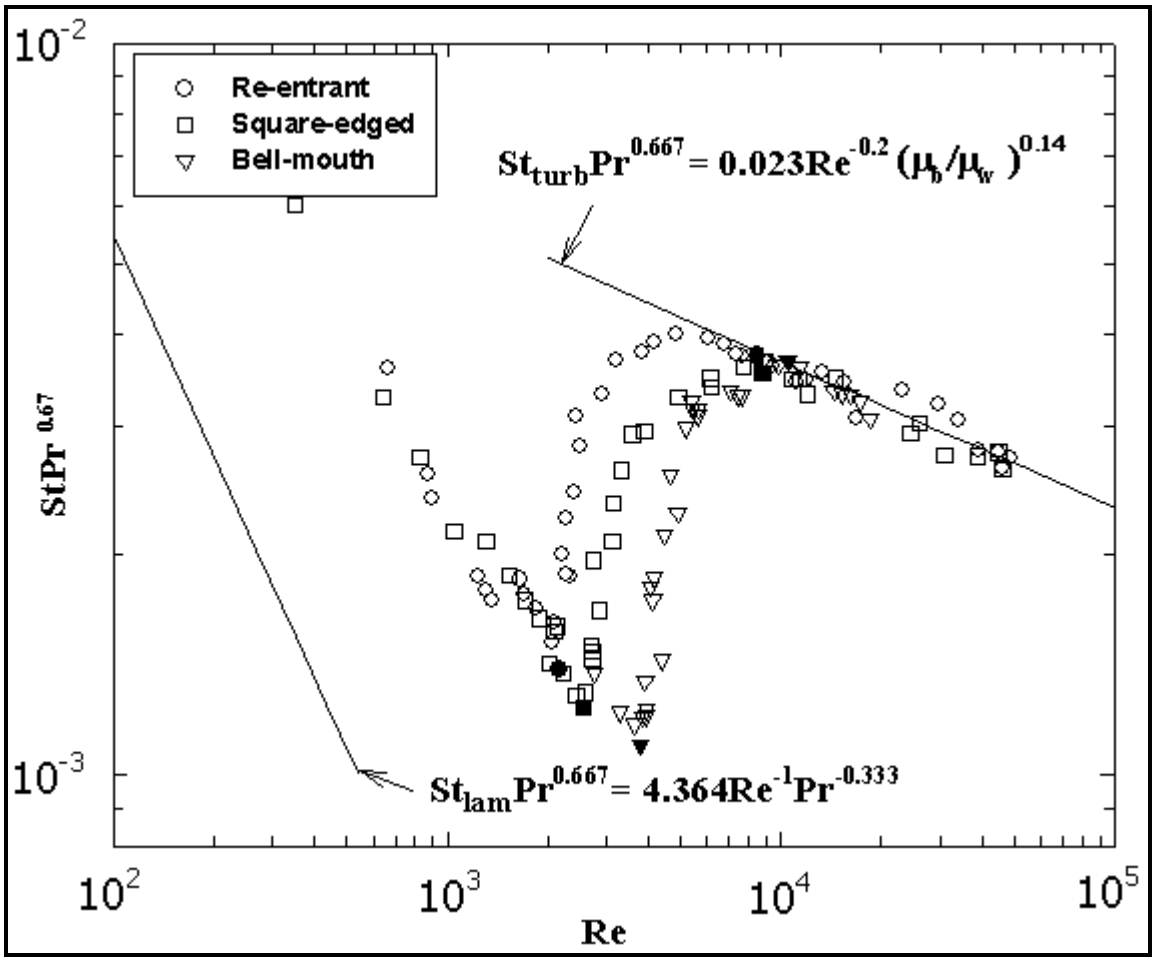

Figure 5.5. Influence of different inlets on the heat transfer transition region at z/D=192 (filled symbols designate the start and end of the transition region for each inlet) between limits of Dittus-Boelter correlation for fully developed turbulent flow (using n = 1/3) and Nu = 4.364 for fully developed laminar flow with a uniform heat flux boundary condition. Note buoyancy effect on the laminar flow data giving the much larger mixed convection heat transfer coefficient. Taken from Ghajar and Tam (1994).

In a subsequent study, Tam and Ghajar (1998) experimentally investigated the behavior of local heat transfer coefficients in the transition region for a tube with a bell-mouth inlet. This type of inlet is used in some heat exchangers mainly to avoid the presence of eddies which are believed to be one of the causes for erosion in the tube inlet region. For the bell-mouth inlet, the variation of the local heat transfer coefficient with length in the transition and turbulent flow regions is very unusual. For this inlet geometry, the boundary layer along the tube wall is at first laminar and then changes through a transition to the turbulent condition causing a dip in the Nu vs. z/d_i curve. In their experiments with a fixed inside

diameter of 15.84 mm (0.624 in.), the length of the dip in the transition region was much longer ($100 < z/d_i < 175$) than in the turbulent region ($z/d_i < 25$). The presence of the dip in the transition region causes a significant influence in both the local and the average heat transfer coefficients. This is particularly important for heat transfer calculations in short tube heat exchangers with a bell-mouth inlet. Figure 5.6 shows the variation of local Nusselt number along the tube length in the transition region for the three inlet configurations at comparable Reynolds numbers.

Ghajar and Madon (1992) and Tam and Ghajar (1997) measured pressure drops in circular plain tubes for fully developed flows in the transition regime for the same three inlet configurations under isothermal and heating conditions, respectively. The widely used expressions for the friction factor f in laminar and turbulent flows with heat and cooling are, respectively:

$$f_{lam} = \left(\frac{16}{Re}\right)\left(\frac{\mu_{bulk}}{\mu_{wall}}\right)^{m} \qquad [5.2.16]$$

$$f_{turb} = \left(\frac{0.0791}{Re^{0.25}}\right)\left(\frac{\mu_{bulk}}{\mu_{wall}}\right)^{m} \qquad [5.2.17]$$

The exponent m for laminar flows depends on a number of factors while for turbulent flows the most typically quoted value is -0.25. In expressions similar to those above for heat transfer, Tam and Ghajar (1997) give the following expression for the transition friction factor f_{trans}:

$$f_{trans} = \left[1+\left(\frac{Re}{A}\right)^{B}\right]^{C}\left(\frac{\mu_{bulk}}{\mu_{wall}}\right)^{m} \qquad [5.2.18]$$

where the exponent m is obtained from:

$$m = m_1 - m_2 Gr^{m_3} Pr^{m_4} \qquad [5.2.19]$$

The values of the empirical constants in this expression are listed in Table 5.1. The range of application of the transition friction factor equation based on their database of 83 points (30 points for the re-entrant inlet, 29 points for the square-edged inlet and 24 points for the bell-mouth inlet) is as follows:

Re-entrant: $2700 \le Re \le 5500$, $16 \le Pr \le 35$, $7410 \le Gr \le 158300$, $1.13 \le \mu_{bulk}/\mu_{wall} \le 2.13$.

Square-edged: $3500 \le Re \le 6900$, $12 \le Pr \le 29$, $6800 \le Gr \le 104500$, $1.11 \le \mu_{bulk}/\mu_{wall} \le 1.89$.

Bell-mouth: $5900 \le Re \le 9600$, $8 \le Pr \le 15$, $11900 \le Gr \le 353000$, $1.05 \le \mu_{bulk}/\mu_{wall} \le 1.47$.

These methods captured about 82% of their data within an error band of ±10% and ±98% of their data with ±20%. For laminar flows with heating, they give the following constants for determining the exponent m in [5.2.16]: $m_1 = 1.65$, $m_2 = 0.013$, $m_3 = 0.170$ and $m_4 = 0.840$, which is applicable over the following range of parameters: $1100 \le Re \le 7400$, $6 \le Pr \le 36$, $17100 \le Gr \le 95600$ and $1.25 \le \mu_{bulk}/\mu_{wall} \le 2.40$.

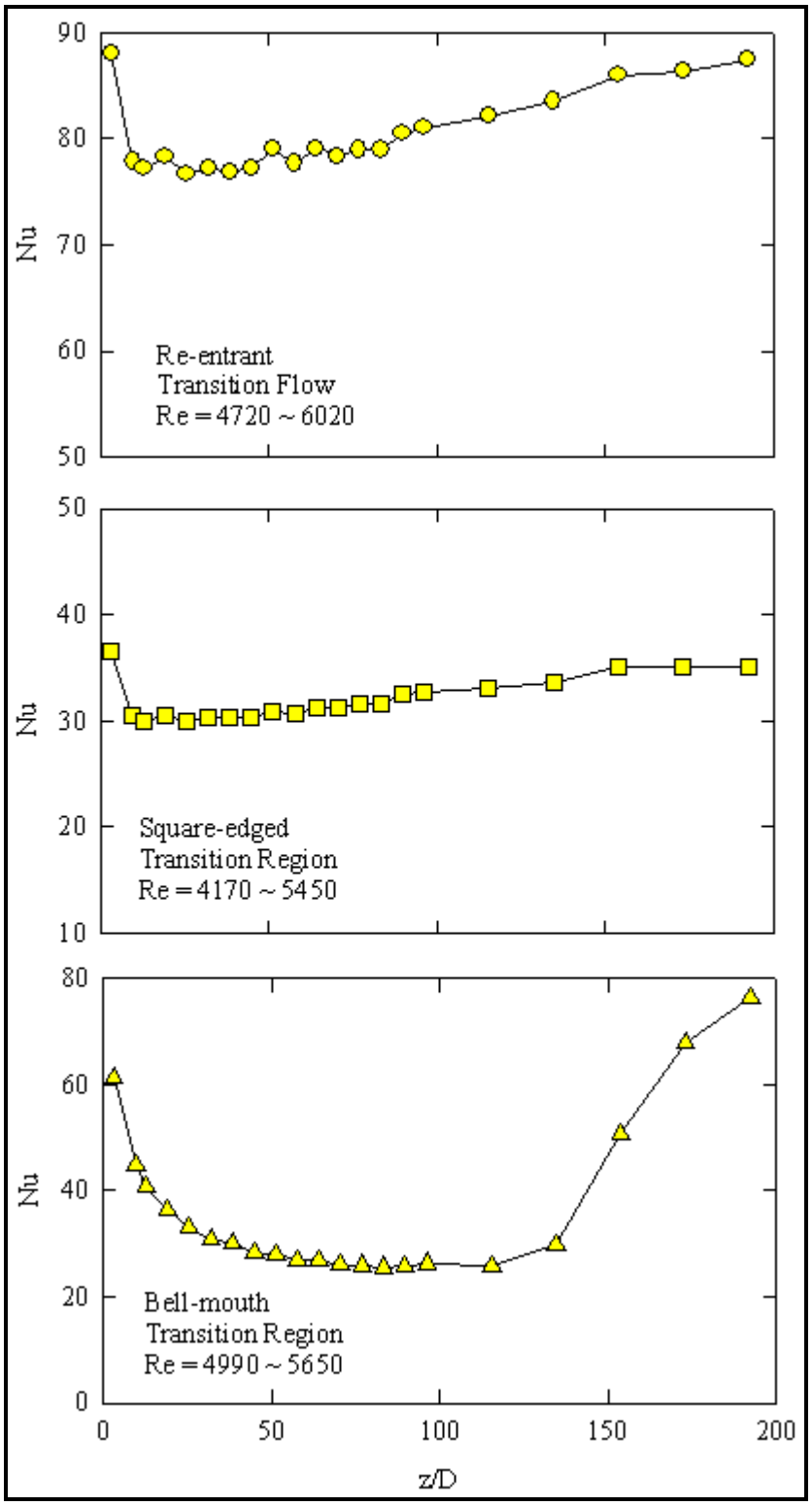

Figure 5.6. Variation of local Nusselt number with length for the re-entrant, square-edged, and bell-mouth inlets in the transition region. Taken from Tam and Ghajar (1998).

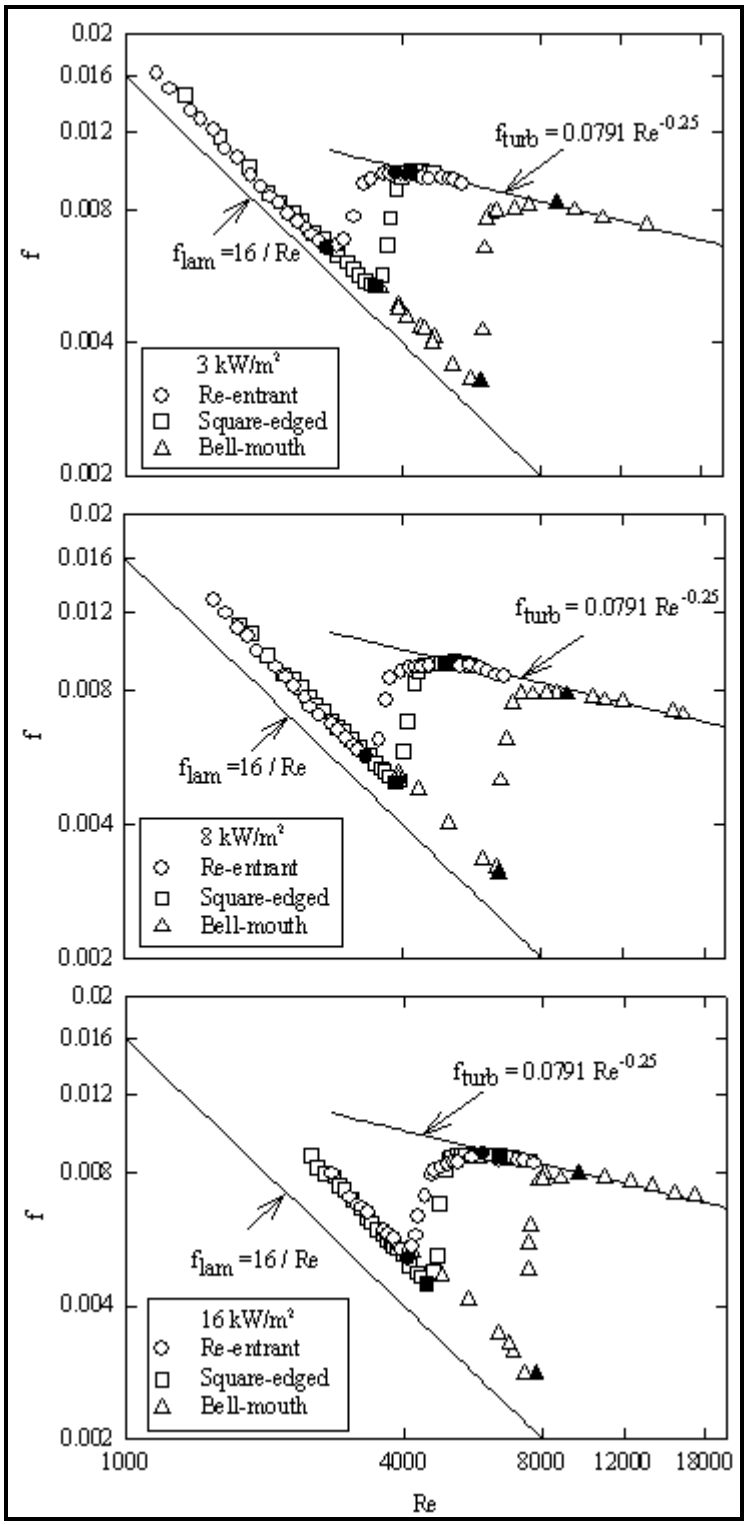

Figure 5.7. Fully developed friction factors for three different inlet configurations and heat fluxes (filled symbols designate the start and end of the transition region for each inlet). Taken from Tam and Ghajar (1997).

The fully developed friction factor results for the three different inlet configurations shown in Figure 5.7 clearly establish the influence of heating rate on the beginning and end of the transition region for each inlet configuration (the filled symbols represent the start and end of the transition region). In the laminar and transition regions, heating seems to have a significant influence on the value of the friction factor. However, in the turbulent region, heating did not affect the magnitude of the friction factor. The significant influence of heating on the values of friction factor in the laminar and transition regions is directly due to the effect of secondary flow.

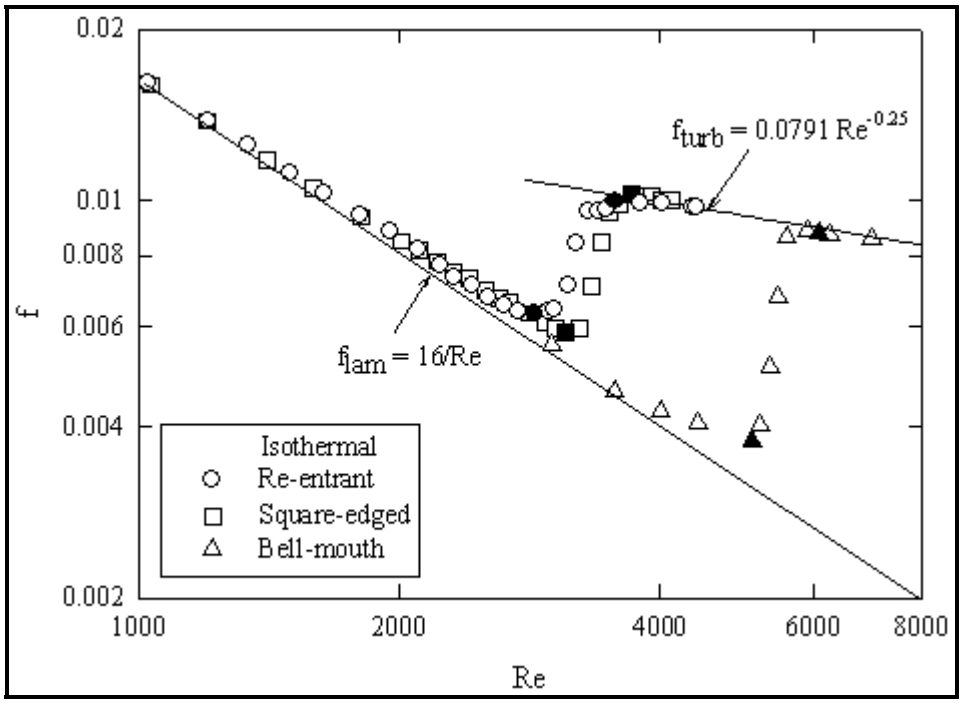

Figure 5.8. Influence of different inlet configurations on the isothermal fully developed friction factors (filled symbols designate the start and end of the transition region for each inlet). Taken from Tam and Ghajar (1997).

According to Tam and Ghajar (1997), the isothermal friction factors for the three inlet types showed that the range of the Reynolds number values at which transition flow exists is strongly inlet geometry dependent. Furthermore, heating caused an increase in the laminar and turbulent friction factors and an increase in the lower and upper limits of the isothermal transition regime boundaries. The transition Reynolds number ranges for the isothermal and non-isothermal (three different heating rates) and the three different inlets used in their study are summarized in Table 5.2. Figure 5.8 shows the influence of inlet configuration on the beginning and end of the isothermal fully developed friction factors in the transition region (the filled symbols represent the start and end of the transition region).

Table 5.2. Transition Reynolds numbers for friction factor.

Type of Inlet: Heat flux	Re-entrant inlet	Square-edged Inlet	Bell-mouth inlet
0 kW/m^2 (adiabatic)	2870< Re < 3500	3100< Re < 3700	5100< Re < 6100
3 kW/m^2	3060< Re < 3890	3500< Re < 4180	5930< Re < 8730
8 kW/m^2	3350< Re < 4960	3860< Re < 5200	6480< Re < 9110
16 kW/m^2	4090< Re < 5940	4450< Re < 6430	7320< Re < 9560

Note that the fully developed friction factors in the laminar, turbulent and transition regions can be easily obtained from [5.2.16], [5.2.17] and [5.2.18], respectively, by setting the exponent on the viscosity ratio correction to unity (i.e. with m = 0).

Example 5.1: Heat transfer in the transition region

Ethylene glycol-distilled water mixture with a mass fraction of 0.6 and a volumetric flow rate of 2.6×10^{-4} m^3/s (4.12 gpm) flows inside a plain tube with an inside diameter of 0.0158 m (0.622 in.) with a uniform wall heat flux boundary condition. For this flow, determine the Nusselt number at the location $z/d_i = 90$ if the inlet configuration of the tube is: (a) re-entrant, (b) square-edged, and (c) bell-mouth. At this location, the local Grashof number is Gr = 51770. The physical properties of ethylene glycol-distilled water mixture at the location of interest are: Pr = 29.2, $\nu = 3.12 \times 10^{-6}$ m^2/s and $\mu_{bulk}/\mu_{wall} = 1.77$.

Solution: For a plain tube with a known diameter and volumetric flow rate, the type of flow regime is determined before making any decision regarding which Nusselt number correlation to use. In this case, the local bulk Reynolds number is calculated with the absolute viscosity evaluated at the fluid bulk temperature:

$$Re = \frac{(Q/A)\, d_i}{\nu} = \frac{[(2.6\times10^{-4}\ m^3/s)/(1.96\times10^{-4}\ m^2)](0.0158\ m)}{3.12\times10^{-6}\ m^2/s} = 6713$$

where $A = \pi d_i^2/4 = 1.96\times10^{-4}\ m^2$

Therefore, the flow regime is in the transition region for all three inlet configurations (thus use Eqs. [5.2.12] to [5.2.14] with $z/d_i = 90$) and therefore Eq. [5.2.9] should be used with the constants a, b, c found in Table 5.1. However, Nu_{lam} and Nu_{turb} are the inputs to Eq. [5.2.9] and they need to be evaluated first from Eqs. [5.2.10] and [5.2.11], respectively. It should be mentioned that the correlations for Nu_{lam} and Nu_{turb} have no inlet dependency.

Applying Eq. [5.2.10]:

$$Nu_{lam} = 1.24\left[\left(\frac{Re\,Pr\,d_i}{z}\right) + 0.025(Gr\,Pr)^{0.75}\right]^{1/3}\left(\frac{\mu_{bulk}}{\mu_{wall}}\right)^{0.14}$$

$$Nu_{lam} = 1.24\left[\left(\frac{(6713)(29.2)}{90}\right) + 0.025[(51770)(29.2)]^{0.75}\right]^{1/3}(1.77)^{0.14} = 19.9$$

Applying Eq. [5.2.11]:

$$Nu_{turb} = 0.023\,Re^{0.8}\,Pr^{0.385}\left(\frac{z}{d_i}\right)^{-0.0054}\left(\frac{\mu_{bulk}}{\mu_{wall}}\right)^{0.14}$$

$$Nu_{turb} = 0.023\,(6713)^{0.8}\,(29.2)^{0.385}\,(90)^{-0.0054}\,(1.77)^{0.14} = 102.7$$

Applying Eq. [5.2.9]:

$$Nu_{trans} = Nu_{lam} + \left\{\exp[(a - Re)/b] + Nu_{turb}^{c}\right\}^{c}$$

For re-entrant inlet:

$$\mathrm{Nu}_{\mathrm{trans}} = 19.9 + \left\{\exp\left[(1766 - 6713)/276\right] + 102.7^{-0.955}\right\}^{-0.955} = 88.2$$

For square-edged inlet:

$$\mathrm{Nu}_{\mathrm{trans}} = 19.9 + \left\{\exp\left[(2617 - 6713)/207\right] + 102.7^{-0.950}\right\}^{-0.950} = 85.3$$

For bell-mouth inlet:

$$\mathrm{Nu}_{\mathrm{trans}} = 19.9 + \left\{\exp\left[(6628 - 6713)/237\right] + 102.7^{-0.980}\right\}^{-0.980} = 21.2$$

It is worth mentioning that for the re-entrant and square-edged inlets, the flow behaves normally. For the bell-mouth inlet, the Nusselt number is low in comparison to the other two inlets. This is because of the unusual behavior of the bell-mouth inlet noted earlier, i.e. the boundary layer along the tube wall is at first laminar and then changes through a transition region to the turbulent condition.

Example 5.2: Non-isothermal fully developed friction factor

A plain tube with a bell-mouth inlet configuration is experiencing an 8 kW/m^2 uniform wall heat flux boundary condition. The tube has an inside diameter of 0.0158 m (0.622 in.) and a volumetric flow rate of 1.32×10^{-4} m^3/s (2.10 gpm). The liquid flowing inside the tube is ethylene glycol-distilled water mixture with a mass fraction of 0.34. Determine the fully developed friction factor at a location along the tube were the Grashof number is Gr = 60800. The physical properties of the ethylene glycol-distilled water mixture at the location of interest are: Pr = 11.6, $\nu = 1.39 \times 10^{-6}$ m^2/s and $\mu_{\mathrm{bulk}}/\mu_{\mathrm{wall}} = 1.14$. Then recalculate the friction factor if a square-edged inlet is used instead.

Solution: For the calculation of the non-isothermal fully developed friction factor, it is necessary to determine the flow regime before making any decision regarding which friction factor correlation should be used. In this case, the local bulk Reynolds number needs to be calculated with the absolute viscosity evaluated at the fluid bulk temperature as follows:

$$\mathrm{Re} = \frac{(\mathrm{Q}/\mathrm{A})\,\mathrm{d_i}}{\nu} = \frac{[(1.32\times10^{-4}\ \mathrm{m^3/s})/(1.96\times10^{-4}\ \mathrm{m^2})](0.0158\,\mathrm{m})}{1.39\times10^{-6}\ \mathrm{m^2/s}} = 7679$$

where $\mathrm{A} = \pi \mathrm{d_i^2}/4 = 1.96\times10^{-4}\ \mathrm{m^2}$

From Table 5.2 for a bell-mouth inlet and a heat flux of 8 kW/m^2, the flow is in the transition region. Therefore, Eq. [5.2.18] with exponent m given by [5.2.19] is applied as follows:

$$f_{\mathrm{trans}} = \left[1 + \left(\frac{\mathrm{Re}}{\mathrm{A}}\right)^{\mathrm{B}}\right]^{\mathrm{C}} \left(\frac{\mu_{\mathrm{bulk}}}{\mu_{\mathrm{wall}}}\right)^{\mathrm{m}}$$

where the constants A, B, C and m are given in Table 5.1. Therefore,

$$f_{\mathrm{trans}} = \left[1 + \left(\frac{\mathrm{Re}}{5340}\right)^{-0.099}\right]^{-6.32} \left(\frac{\mu_{\mathrm{bulk}}}{\mu_{\mathrm{wall}}}\right)^{-2.58 - 0.42\mathrm{Gr}^{-0.41}\mathrm{Pr}^{2.46}}$$

$$f_{trans} = \left[1 + \left(\frac{7679}{5340}\right)^{-0.099}\right]^{-6.32} (1.14)^{-2.58-0.42\times 60800^{-0.41}\times 11.6^{2.46}} = 0.0078$$

Resolving the problem with a square-edged inlet. For this inlet shape, the Reynolds number of the flow is the same as that of the bell-mouth inlet (Re = 7679). However, it is necessary to check the type of flow regime for this particular inlet with 8 kW/m^2 of heating. According to Table 5.2, the transition Reynolds number range for this case is 3860 < Re < 5200, which means that the flow in this case is turbulent and [5.2.17] is the appropriate equation to use:

$$f_{turb} = \left(\frac{0.0791}{Re^{0.25}}\right)\left(\frac{\mu_{bulk}}{\mu_{wall}}\right)^{m} = \left(\frac{0.0791}{7679^{0.25}}\right)(1.14)^{-0.25} = 0.0082$$

5.3 Mechanisms of Turbulent Heat Transfer Augmentation

Extended Surface Area. One way to increase turbulent heat transfer coefficients is to increase the surface area in contact with the fluid to be heated or cooled. Some enhancement correlations incorporate a surface area ratio factor to account for this effect while others do not. It is common practice to develop heat transfer correlations for internal flows in enhanced tubes based on the internal ***nominal*** surface area, i.e. that of the perimeter of the maximum internal diameter of the tube d_i (corrugations) or at the base of any internal enhancement (fins or ribs) [***all correlations in this chapter follow this format***]. This heat transfer coefficient is used directly in calculating the overall heat transfer coefficient at this diameter without use of a surface area ratio. It is *not* common practice to reduce single-phase turbulent flow heat transfer data relative to the total internal surface area. If internal fin efficiency becomes important, it is thus difficult to determine the effect from nominal internal area correlations. However, commonly used fins and ribs are quite small in height compared to external fins and their fin efficiencies are normally over 0.95 while for copper tubes they approach 0.99. Since the original experimental data would normally have been reduced to a heat transfer correlation without correcting for fin efficiency, this effect is already incorporated for tubes of that same material. Thus, any effect of fin efficiency can normally be safely ignored. On the other hand, twisted tape inserts normally fit loosely inside a tube (thus they have poor thermal contact to the inner tube wall) and hence the surface area of a twisted tape is not considered to be heat transfer surface area, only that of the plain tube perimeter in which it is installed.

Surface Roughness. The internal roughness of the tube surface is well known to increase the turbulent heat transfer coefficient. Normally, a smooth internal surface of a tube is assumed in design, as in all the correlations presented above. However, the Churchill (1983) correlation can be solved for the friction factor of rough tubes with a commercial pipe roughness of e:

$$\sqrt{\frac{2}{f}} = -2.46 \ln\left[\frac{e}{d_i} + \left(\frac{7}{Re}\right)^{0.9}\right] \qquad [5.3.1]$$

This form of friction factor correlation has also been modified for predicting heat transfer and pressure drop in enhanced tubes as will be seen later and works in conjunction with [5.2.7].

Swirl. Swirl of the flow is also known to augment heat transfer. Internal helical fins or ribs, corrugations and twisted tapes impart a swirl effect on the fluid. This tends to increase the effective flow length of the fluid through the tube, which increases heat transfer and pressure drop. For internal helical fins, ribs and

corrugations however, the effect of swirl tends to decrease or disappear all together at higher helix angles since the fluid flow then simply passes axially over the fins or ribs. For twisted tape inserts, the effect of swirl on augmentation plays an important role.

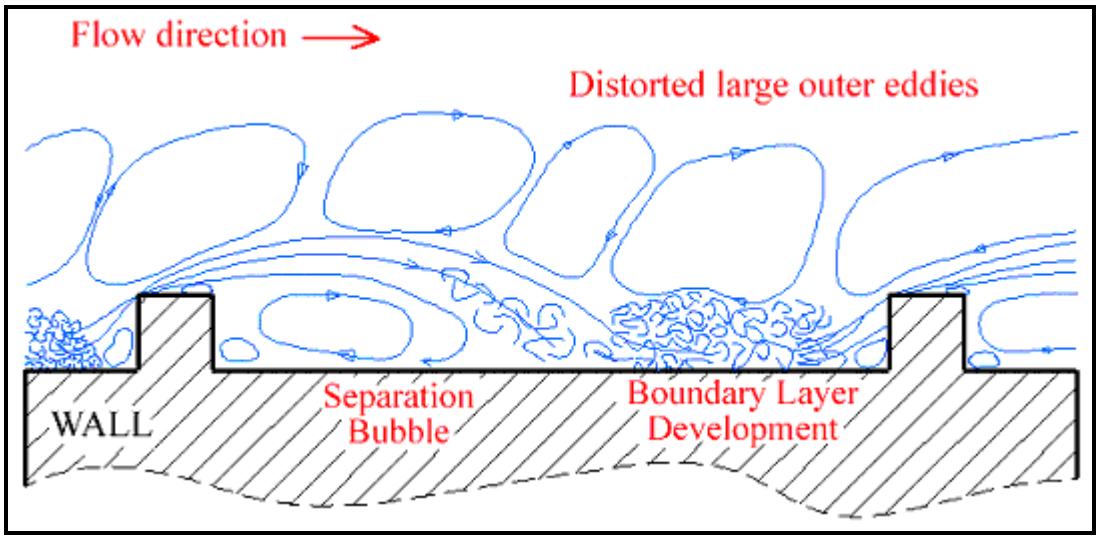

Figure 5.9. Turbulent flow structure over a two-dimensional rib from Rabas and Arman (1992).

Boundary Layer Displacement. The displacement of the turbulent boundary layer is a particularly important heat transfer mechanism for augmenting heat transfer. Figure 5.9 depicts a diagram that Rabas and Arman (1992) use to illustrate this process. For essentially a two-dimensional flow, it shows the separation of the flow as it passes over a transverse rib (creating a small recirculation zone in front of the rib), the formation of a recirculation zone behind the rib, flow reattachment on the base wall and then flow up and over the next rib. Recirculation eddies are formed above these flow regions. Rabas and Arman commented as follows on a rib's effect on the heat transfer process:

- There are six distinct heat transfer regions, although some are more important than others (the upstream recirculation zone, the rib's upstream, top and downstream faces, the downstream recirculation zone, and finally the boundary layer reattachment/redevelopment zone);
- Two peaks in local heat transfer occur, one at the top of the rib and the other in the downstream recirculation zone just before the reattachment point;
- Heat transfer enhancement increases substantially with increasing Prandtl number, so that for large Pr fluids heat transfer is dominated by flow around the rib surfaces;
- The surface-averaged heat transfer performance is directly proportional to the maximum enhancement at the rib;
- The point of the local maximum in the heat transfer coefficient on the base wall between ribs moves upstream towards the back of the rib with increasing Reynolds and Prandtl numbers, and is located on the base wall between the reattachment point and the point of maximum wall shear stress;
- The Prandlt number has the same influence on thermal performance in the downstream recirculation region as at the rib;
- The high heat transfer augmentation in the downstream recirculation region is due to the high turbulence levels near the surface;
- Two more local maximums in heat transfer occur at large Reynolds roughness numbers in the front recirculation zone before the rib and on the rear face of the rib.

Webb, Eckert and Goldstein (1971) have presented an interesting composite diagram of the recirculation and reattachment zones as a function of rib spacing for ribs oriented normal to the flow. Figure 5.10 shows this diagram where the flows are characterized by the axial rib pitch to rib height (p/e) ratio. For closely spaced ribs (at bottom of diagram), one large recirculation eddy is trapped between two successive ribs with two small eddies in the corners. As the p/e ratio increases, the large recirculation eddy elongates until it is broken and a reattachment zone is formed, such that two dominant eddies exist at larger ratios.

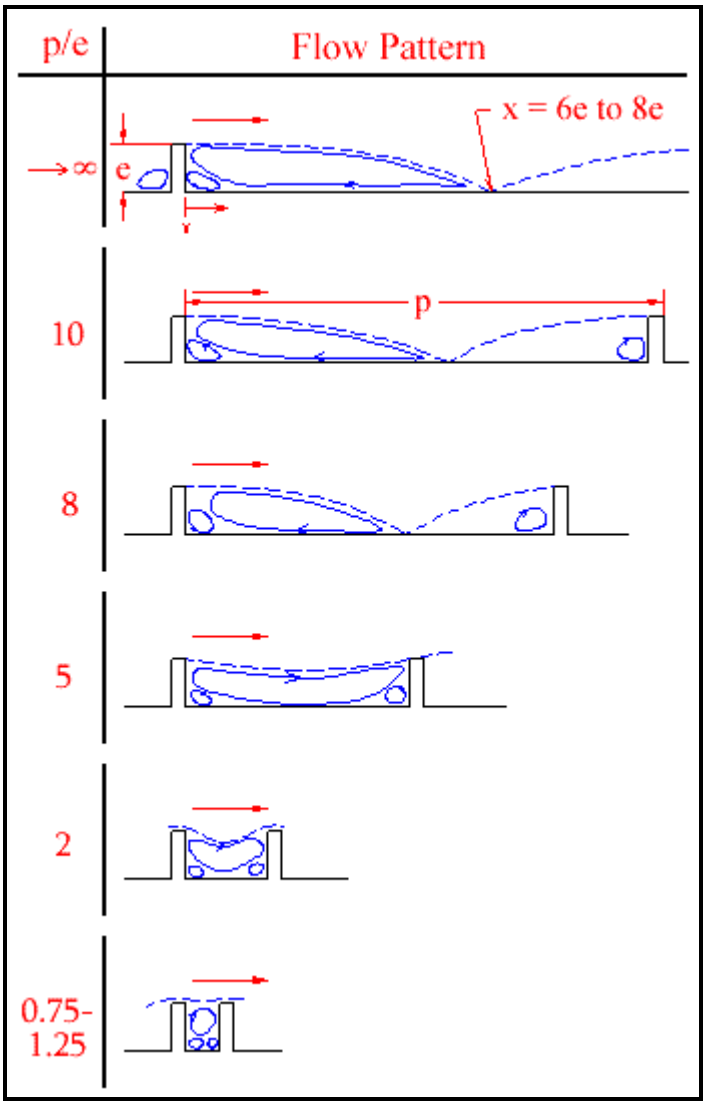

Figure 5.10. Recirculation flow patterns over transverse ribs as a function of rib spacing from Webb, Eckert and Goldstein (1971).

5.4 Turbulent Heat Transfer with Twisted Tape Inserts

A schematic diagram of a twisted tape insert inside a tube is shown in Figure 5.11. The enhancement is defined geometrically by the thickness of the tape δ and its twist ratio, y. The twist ratio is defined as the axial length for a *180°* turn of the tape divided by the internal diameter of the tube. ***This is the most***

common definition used in research literature and that used here. It is also common to use the axial length for a complete *360°* turn instead in commercial literature; hence, double-check the definition used before applying a twisted tape prediction method or using experimental results from manufacturer's literature or a scientific publication and then make sure to indicate the definition used in the resulting heat exchanger specification sheet.

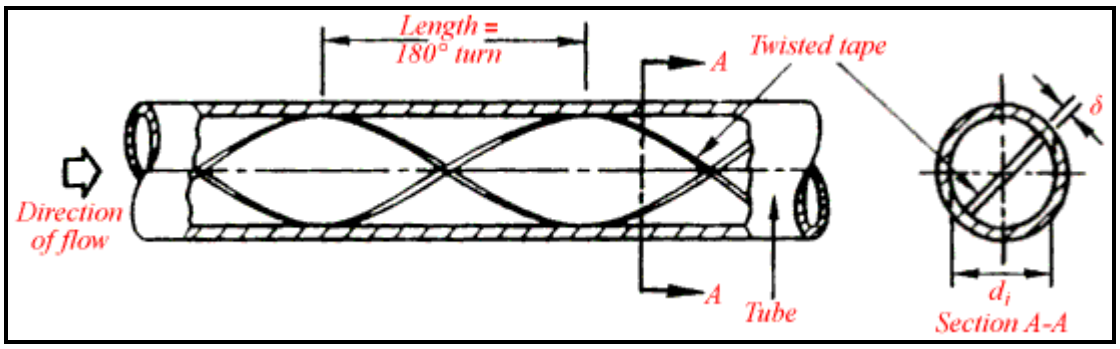

Figure 5.11. Diagram of a twisted tape insert inside a tube.

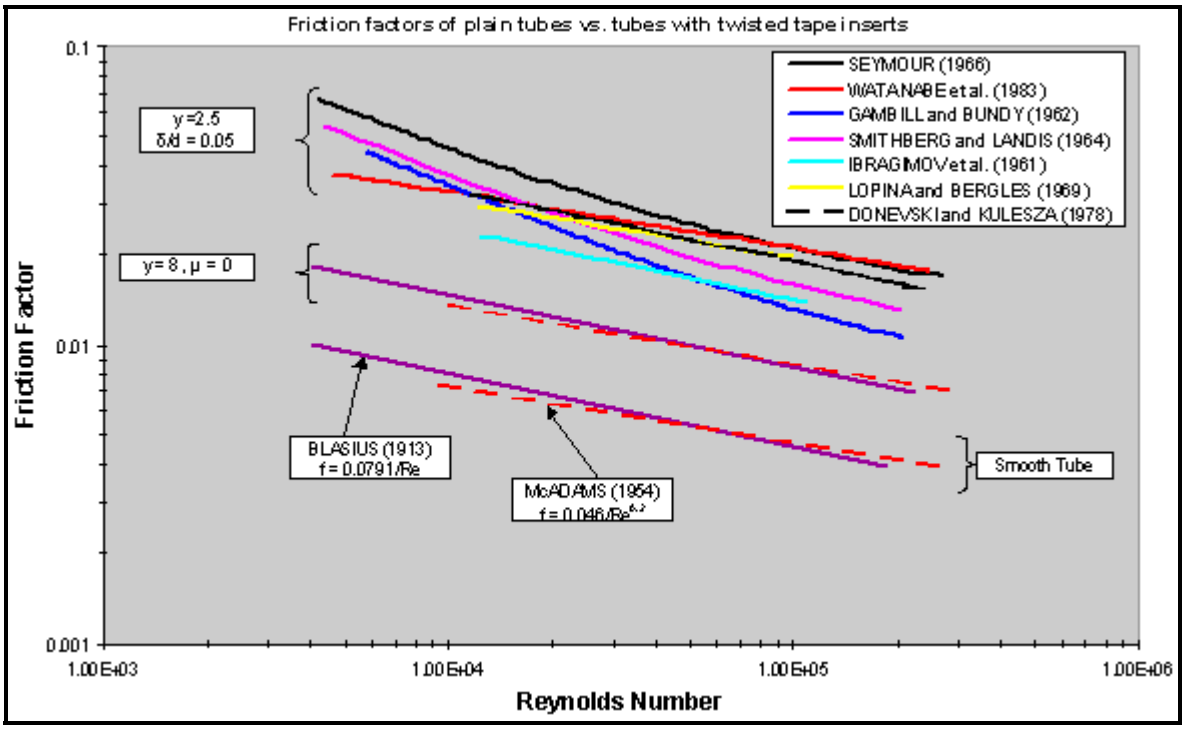

Figure 5.12. Isothermal friction factors in plain tubes with and without tape inserts.

Numerous experimental studies have investigated turbulent flow heat transfer with twisted tape inserts and proposed heat transfer and pressure drop prediction methods. Manglik and Bergles (1992) have presented composite graphs of these prediction methods from selected studies. Figure 5.12 depicts the friction factor correlations for a smooth tube, those of Blasius (1913) and McAdams (1954), that for flow in a half-tube ($y = \infty$, $\delta = 0$) based on its hydraulic diameter, and those from seven studies evaluated for the same choice of twisted tape ($y = 2.5$, $\delta/d_i = 0.05$). First of all, one sees that an important part of the increase in friction factor (based on the internal tube perimeter for all cases) is caused by the flow being

divided into two smaller flow channels. That is, compare the plain tube curves to those for flow in the tube whose cross-section is divided by an infinitesimally thin wall. Secondly, one sees that the effect of the swirl and longer flow path for the tape results in a second important increase in friction factor. The methods presented demonstrate a significant discrepancy in their predictions with one another.

Figure 5.13 and Figure 5.14 depict the Nusselt number predictions from the same studies, evaluated for air and water, respectively. The Nusselt numbers have been divided by the bulk-to-wall viscosity ratio, Prandtl number ratio or temperature ratio to correct for physical property effects for the particular method to remove this effect from the graph. For air, there is reasonable agreement between the prediction methods, except for the method of Ibragimov, Nomofelov and Subbotin (1961). The level of augmentation starts out at about a factor of two at the lower Reynolds numbers and tends to decrease with increasing Reynolds number. For water, the level of augmentation also starts out at about a factor of two at the lower Reynolds numbers and tends to decrease with increasing Reynolds number. There is a larger divergence between the prediction methods for water than for air.

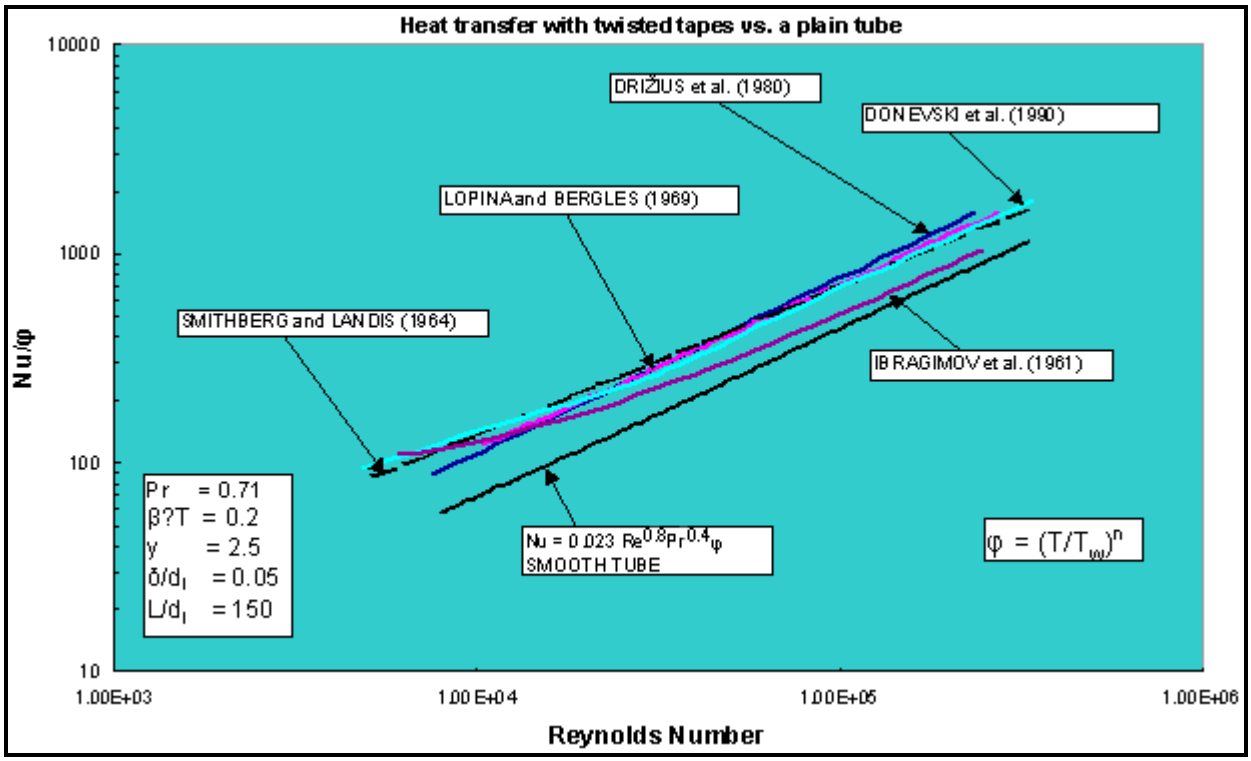

Figure 5.13. Nusselt numbers in plain tubes with and without tape inserts for air.

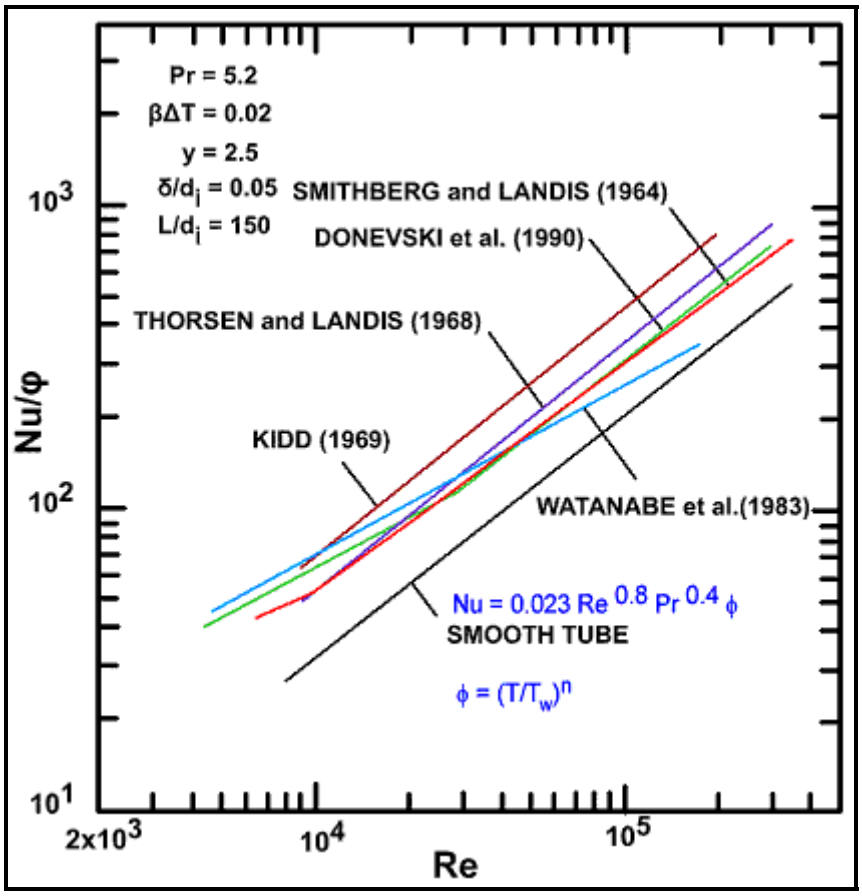

Figure 5.14. Nusselt numbers in plain tubes with and without tape inserts for water.

Manglik and Bergles (1992) proposed the following friction factor correlation for tubes with twisted tape inserts and is the recommended method here for general use:

$$f = \frac{0.0791}{\mathrm{Re}^{0.25}}\left[\frac{\pi}{\pi - 4(\delta/d_i)}\right]^{1.75}\left[\frac{\pi + 2 - 2(\delta/d_i)}{\pi - 4(\delta/d_i)}\right]^{1.25}\left[1 + \frac{2.752}{y^{1.29}}\right] \qquad [5.4.1]$$

The value of Re in this expression is based on the flow in the tube without the insert, i.e. bare tube Reynolds number as in [5.2.2], y is the twist ratio based on the axial length for a 180° turn, δ is the thickness of the tape and d_i is the internal diameter of the bare tube. This expression described within about ±5% most of the friction factor data available in the literature covering twist ratios from about 2.5 to 10, which are of most industrial interest. Their corresponding heat transfer correlation for turbulent flows gives the twisted tape Nusselt number as:

$$\frac{\mathrm{Nu}_{tt}}{\mathrm{Nu}_{y=\infty}} = 1 + \frac{0.769}{y} \qquad [5.4.2]$$

where the Nusselt number for the twisted tape Nu_{tt} is defined as:

$$Nu_{tt} = \frac{\alpha_{tt} d_i}{k} \qquad [5.4.3]$$

The Nusselt number for a straight tape without twist (y = ∞) is:

$$Nu_{y=\infty} = 0.023\,Re^{0.8}\,Pr^{0.4}\left[\frac{\pi}{\pi - 4(\delta/d_i)}\right]^{0.8}\left[\frac{\pi + 2 - 2(\delta/d_i)}{\pi - 4(\delta/d_i)}\right]^{0.2} J_\mu \qquad [5.4.4]$$

The physical property correction factor J_μ for liquids is given by

$$J_\mu = \left(\frac{\mu_{bulk}}{\mu_{wall}}\right)^n \qquad [5.4.5]$$

The exponent n is equal to 0.18 for liquid heating and 0.30 for liquid cooling. The correction factor for gases is:

$$J_\mu = \left(\frac{T_{bulk}}{T_{wall}}\right)^m \qquad [5.4.6]$$

Many publications also refer to J_μ as φ. The exponent m is equal to 0.45 for gas heating and 0.15 for gas cooling. The method predicts most of their experimental results to within ±10% and covers twist ratios from about 2.5 to 10 (based on the 180° definition).

Some other studies of interest on twisted tapes are: Gambill and Bundy (1962), Smithberg and Landis (1964), Seymour (1966), Thorsen and Landis (1968), Kidd (1969), Lopina and Bergles (1969), Drizius, Shkema and Shlanciauskas (1980), Watanabe, Taira and Mori (1983) and Donevski et al. (1990).

5.5 Turbulent Heat Transfer in Corrugated Tubes

A significant number of corrugated tube types have been tested over the years. For example, Withers (1980a, 1980b) investigated 14 configurations for water, Li et al. (1982) studied 20 configurations for water, Sethumadhavan and Rao (1986) tested 5 configurations for water-glycerine and Mehta and Rao (1988) looked at 11 configurations for water. Withers (1980a) gave the following design methods for Wolverine Korodense tubes applicable to water in the range $10^4 < Re < 10^5$ and temperatures below 88°C (190°F). His friction factor correlation was developed by modifying a rough tube correlation to obtain:

$$\sqrt{\frac{2}{f}} = -2.46 \ln\left[r + \left(\frac{7}{Re}\right)^m\right] \qquad [5.5.1]$$

His correlation for the heat transfer coefficient α_{ct} for Wolverine Korodense tubes is obtained from the following dimensional equation in U.S. units:

$$\alpha_{ct} = \frac{c_p \dot{m} \sqrt{f/2}}{\beta_{ct} \, \mathrm{Pr}\left(\mathrm{Re}\sqrt{f/2}\right)^{0.127} + \gamma} \qquad [5.5.2]$$

Re is the plain tube Reynolds number based on the maximum internal diameter of the corrugated tube d_i and Pr is the Prandtl number. The resulting heat transfer coefficient is in Btu/h ft^2°F, the specific heat is in Btu/lb°F and the mass velocity is in lb/h ft^2. For the Korodense type MHT tube, the values of the design constants are: m = 0.44, r = 0.00595 and γ = 2.56. This class of Korodense tube has a medium corrugation severity. For the Korodense type LPD tube, the values of the design constants are: m = 0.61, r = 0.00088 and γ = 3.74. This class of Korodense tube has a lower corrugation severity and has a pressure drop of about ½ that of MHT but with lower thermal performance by about 25%. Hence, the user can choose the most appropriate version for his application. The value of his empirical constant β_{ct} is specific to each tube size and tube type. It varies in value from about 5.0 to 7.2 for specific tube part numbers with 6.0 a medium value for all. The actual values for these parameters can be found in the appropriate *Wolverine Engineering Databook II* table on Korodense tubes. The friction factor is placed in equation [5.2.7] to calculate the pressure drop for a corrugated tube of length L.

Example 5.3: Heat transfer and pressure drop in a corrugated tube

For a liquid flowing inside a corrugated tube (Korodense type MHT), determine the local heat transfer coefficient and pressure drop at a mass velocity is 500 kg/m^{2}s assuming the internal diameter is 15.75 mm (0.620 in.) and the tube length is 3 m (9.84 ft). The physical properties of the fluid are: ρ = 997 kg/m^3; μ_{bulk} = 0.0007 Ns/m^2; μ_{wall} = 0.0005 Ns/m^2; k = 0.6 W/m K; c_p = 4200 J/kg K; Pr = $c_p\mu/k$ = 4.9.

***Solution*:** For the Korodense type MHT tube, the values of the design constants are: m = 0.44, r = 0.00595 and γ = 2.56. The value of the empirical constant β_{ct} is assumed to be 6.0. The Reynolds number Re is determined using [5.2.2] as:

$$\mathrm{Re} = \frac{\dot{m} d_i}{\mu} = \frac{500(0.01575)}{0.0007} = 11250$$

The friction factor is obtained from [5.5.1]:

$$\sqrt{\frac{2}{f}} = -2.46 \ln\left[\mathrm{r} + \left(\frac{7}{\mathrm{Re}}\right)^{\mathrm{m}}\right] = -2.46 \ln\left[0.00595 + \left(\frac{7}{11250}\right)^{0.44}\right]$$

$$\sqrt{f/2} = 0.1309$$

Applying the viscosity ratio correction of $(\mu_{bulk}/\mu_{wall})^{-0.25}$ = 0.919, this value becomes 0.1260. The correlation for the heat transfer coefficient α_{ct} for Korodense tubes is in U.S. units, so that c_p = 4200 J/kg K = 1.003 Btu/lb°F and the mass velocity is 367905 lb/h ft^2. From [5.5.2] and applying the viscosity ratio correction factor:

$$\alpha_{ct} = \frac{c_p \dot{m}\sqrt{f/2}}{\beta_{ct}\,\mathrm{Pr}\left(\mathrm{Re}\sqrt{f/2}\right)^{0.127} + \gamma}\left(\frac{\mu_{bulk}}{\mu_{wall}}\right)^{0.14}$$

$$= \frac{1.003(367905)(0.1260)}{6.0(4.9)(11250(0.1260))^{0.127} + 2.56}\left(\frac{0.0007}{0.0005}\right)^{0.14}$$

$$\alpha_{ct} = 637.5\ \mathrm{Btu/h\,ft^2\,°F} = 3620\ \mathrm{W/m^2K}$$

The pressure drop in a tube of length L = 3.0 m is obtained by first determining the friction factor and then applying [5.2.7] to obtain:

$$\Delta p = \frac{2f\dot{m}^2 L}{\rho d_i} = \frac{2(0.03175)(500^2)(3.0)}{(997)(0.01575)} = 3033\ \mathrm{Pa}$$

5.6 Turbulent Heat Transfer in Internally Finned or Ribbed Tubes

Withers (1980b) proposed methods for internally helically finned (or ribbed or ridged) Wolverine Turbo-Chil and S/T Trufin tubes that are similar to those he developed for corrugated tubes. In fact, the same friction factor expression [5.5.1] is assumed but uses different values of the empirical constants r and m. His correlation for the heat transfer coefficient α_{ft} for these tubes is obtained from the following dimensional equation that is slightly different than [5.5.2]:

$$\alpha_{ft} = \frac{c_p \dot{m}\sqrt{f/2}}{\beta_{ft}\,\mathrm{Pr}\left(\mathrm{Re}\sqrt{f/2}\right)^{0.136} + \gamma} \qquad [5.6.1]$$

Here, Re is the plain tube Reynolds number based on the maximum internal diameter of the internally finned tube, d_i, which is the root diameter at the base of internal fins. The resulting heat transfer coefficient is in Btu/h ft^2°F, the specific heat is in Btu/lb°F and the mass velocity is in lb/h ft^2. For internally finned tubes, the possible values of r are 0.0, -0.0004, -0.0022 and -0.0020 depending on the particular tube size and wall thickness. Depending on the particular tube, the values of the correction factor β_{ft} range from about 4.43 to 4.72, the values of γ range from about 3.31 to 5.34, and the values of exponent m for the friction factor expression range from 0.58 to 0.73. Specific values for these parameters can be found in the *Wolverine Engineering Databook II* table on Turbo-Chil Characteristics for a particular tube.

For Wolverine Turbo-B types of tubes, the internal heat transfer coefficient is correlated relative to the dimensionless Sieder and Tate (1936) turbulent flow heat transfer equation by changing the leading constant, so that:

$$\frac{\alpha_{ft}\, d_i}{k} = C_{fth}\,\mathrm{Re}^{0.8}\,\mathrm{Pr}^{1/3}\left(\frac{\mu_{bulk}}{\mu_{wall}}\right)^{0.14} \qquad [5.6.2]$$

where the correlation is based on the maximum internal tube diameter d_i and α_{ft} is the heat transfer coefficient. In this expression, C_{fth} is the empirical leading constant in place of the normal plain tube

value of 0.027. Note that this correlation uses the Prandtl number to the 1/3 power, $Pr^{1/3}$. For the original Turbo-B tube version, C_{fth} is equal to 0.060 for 19.05 mm (3/4 in.) tubes and is equal to 0.061 for 25.4 mm (1 in.) versions. The frictional pressure drop is fit by a Blasius type expression:

$$f = \frac{C_{ft}}{Re^{D}} \qquad [5.6.3]$$

Here, the values of C_{ft} and D are required and depend on the tube type. For instance, for the 19.05 mm (¾ in.) original Turbo-B version, C_{ft} = 0.198 and D = 0.267. Re is based on equation [5.2.2] using the maximum internal tube diameter for d_i.

Arman and Rabas (1992) studied the effect of the specific two-dimensional disruption shape on heat transfer and friction factor using a non-orthogonal, body-fitted numerical code. Figure 5.15 depicts the disruption shapes they considered: semicircular, trapezoidal, sine and arc. They presented graphs showing the local variation in wall shear stress and heat transfer for these geometries and a tabular summary of results. Interestingly, they did not find a large difference in mean heat transfer performance in comparisons at equal e/p ratios, where e is the height of the disruption and p is the axial pitch. The trapezoidal shape gave the best performance but only on the order of 10% better than the others.

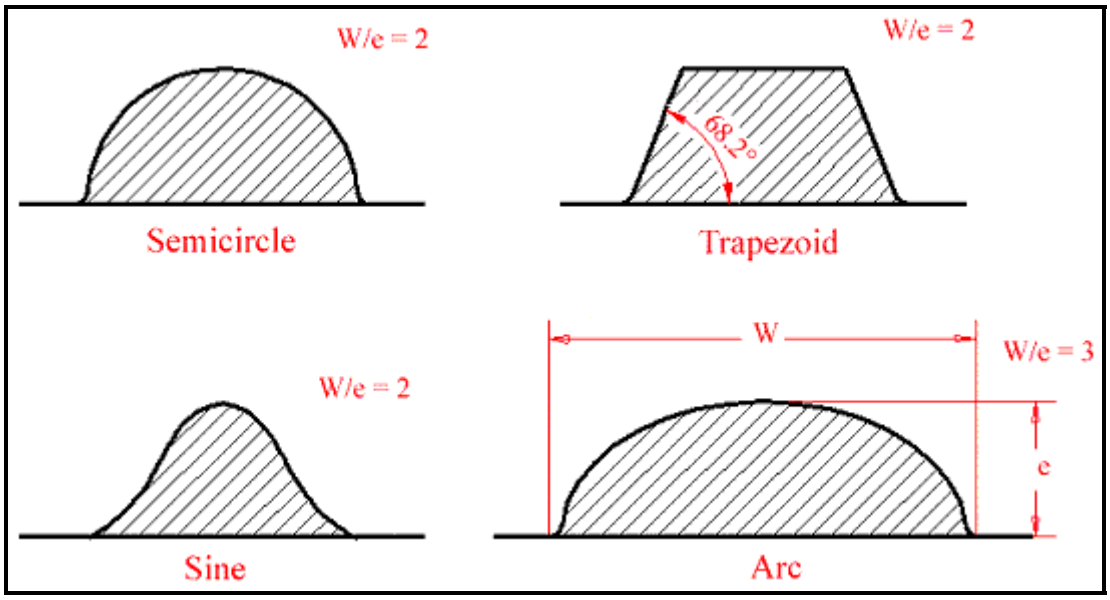

Figure 5.15. Disruption shapes considered by Arman and Rabas (1992).

Nunner (1956) apparently did the first systematic experimental investigation on the effect of disruption shape on heat transfer and friction factor. For four tubes plus one plain tube, the experiments were conducted on three different shapes and two different p/e ratios. The cross-sectional shapes were essentially square (p/e = 20), hemispherical (p/e = 20 and 80) and arc (p/e = 80). Figure 5.16 presents curve fits to their Nusselt numbers for these disruption shapes while Figure 5.17 shows the corresponding friction factors for these disruption shapes. The graphs cover both laminar and turbulent flows. For the latter at Re > 2300, the square shape has the highest heat transfer performance but also the highest friction factor.

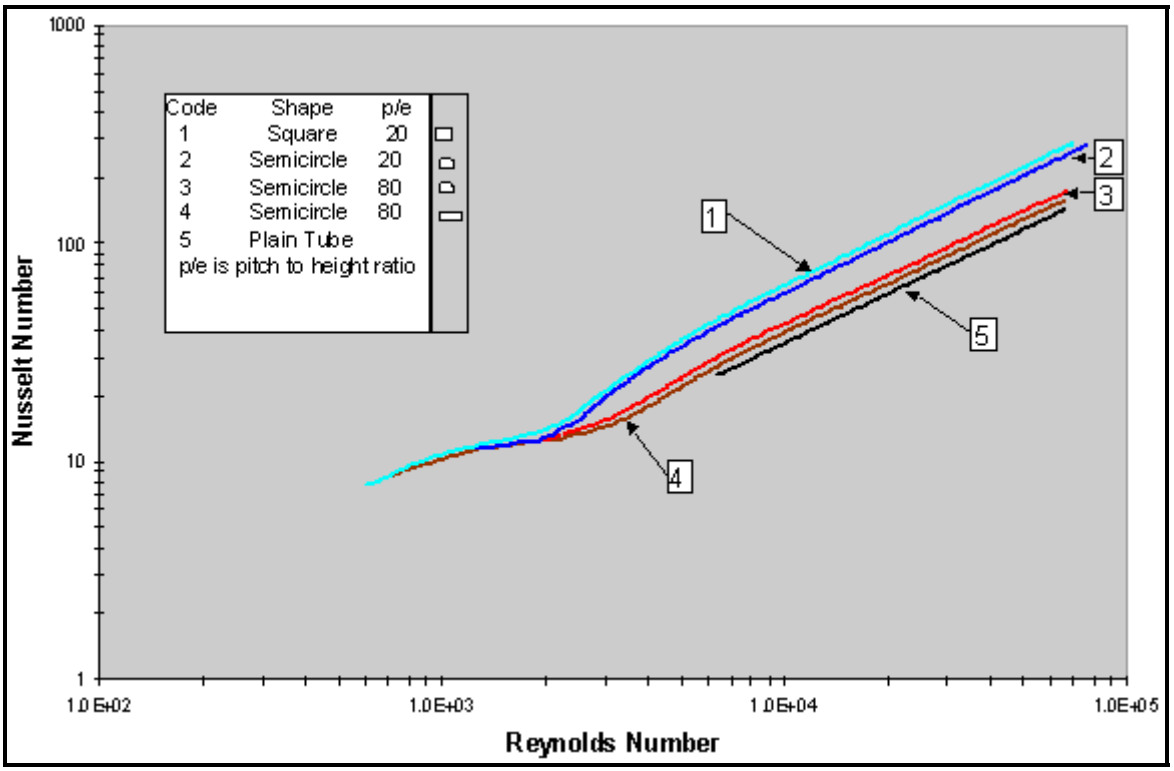

Figure 5.16. Heat performance of disruption shapes from Nunner (1956).

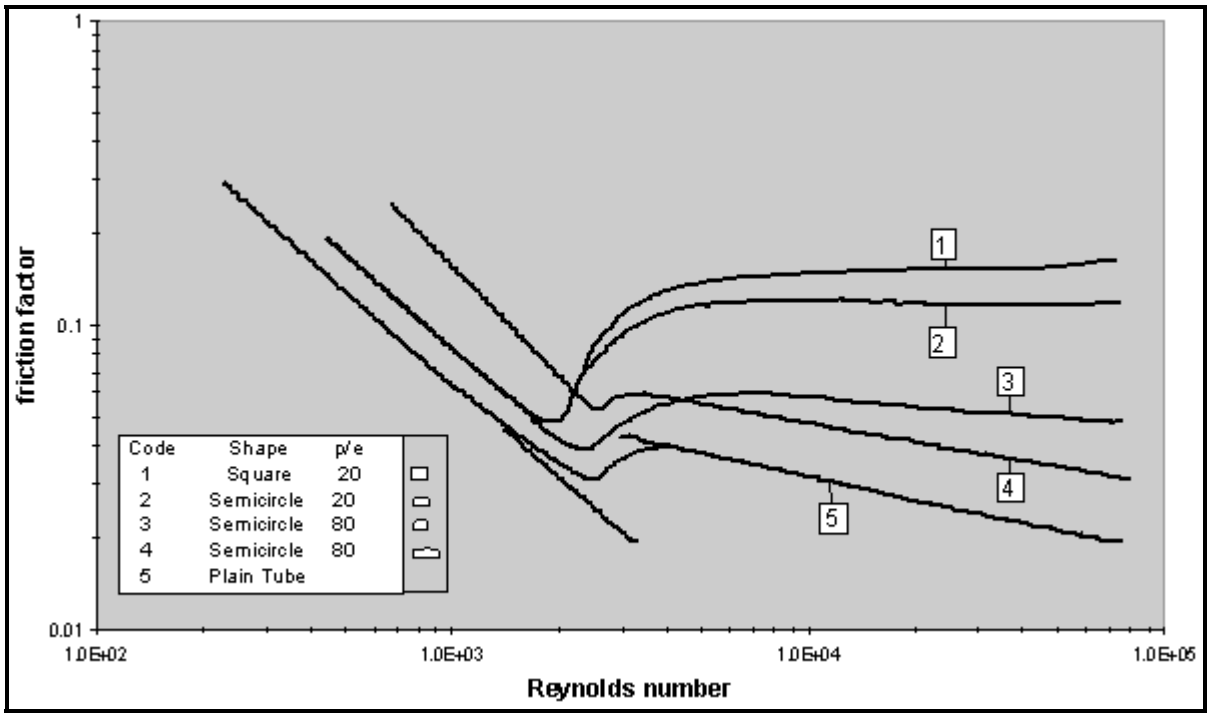

Figure 5.17. Friction factors of disruption shapes from (1956).

Carnavos (1979) proposed heat transfer and friction factor correlations for internally finned tubes in the turbulent flow regime based on experimental tests with 21 tube geometries, including axial fins and helical fins up to 30°. His database covered tests with air, water and an ethylene glycol/water mixture. His heat transfer correlation is:

$$\frac{Nu_{ft}}{Nu_{D-B}} = \frac{\alpha_{ft} d_h / k}{\alpha_{pt} d_i / k} = \left[\frac{d_i}{d_{im}} \left(1 - \frac{2e}{d_i} \right) \right]^{-0.2} \left(\frac{d_i d_h}{d_{im}^2} \right)^{0.5} \sec^3 \beta \qquad [5.6.4]$$

In this correlation, Nu_{D-B} is the plain tube Nusselt number given by the Dittus-Boelter equation [5.2.1] where Re in that expression is based on equation [5.2.2] using the maximum internal tube diameter for d_i. The hydraulic diameter d_h is the given by:

$$d_h = \frac{4A_{fa}}{A_a} \qquad [5.6.5]$$

where A_{fa} is the actual free flow cross-sectional area in m^2 and A_a is the actual heat transfer area per unit length in m^2/m. The meltdown internal diameter d_{im} in the above expression is that which would exist if the fins were melted down and added to the internal perimeter of the tube. The helix angle of the fins with respect to the axis of the tube is β. His corresponding friction factor expression is:

$$\frac{f_{ft}}{f_{Blasius}} = \frac{d_{im}}{d_i} \sec^{0.75} \beta \qquad [5.6.6]$$

This expression gives the finned tube friction factor relative to the Blasius (1913) friction factor equation for a plain, smooth tube:

$$f_{Blasius} = \frac{0.046}{Re^{0.2}} \qquad [5.6.7]$$

Re is based on equation [5.2.2] using the maximum internal tube diameter for d_i. These correlations fit his database to within about ±10%. This expression does not cover helix angles above 30° and it does *not* extrapolate well to higher values. It is applicable to $10^4 < Re < 10^5$ and $0.7 < Pr < 30$. The finned tube friction factor obtained with [5.6.6] can be placed in equation [5.2.7] to calculate the pressure drop for an internally finned tube of length L.

Ravigururajan and Bergles (1985) have proposed what is here considered to be the most general and accurate method for predicting heat transfer and pressure drop inside internally ribbed tubes (and plain tubes with coiled wire inserts). Their method is also applicable to most internally finned tubes and is hence given in this section and uses the same nomenclature as the methods above. Figure 5.18 depicts the rib geometries and profiles (and wire geometry) that they included in their study where e is the height of the rib or diameter of the wire, p is the axial pitch from one rib (or wire) to the next, β is the helix angle of the rib or wire relative to the tube axis, β_{rib} is the profile contact angle of the rib to the internal surface of the tube and $n_{corners}$ is the number of sharp corners of the rib facing the flow (two for triangular or rectangular cross-section ribs and infinity for smoother profiles). The profile contact angle for a circular sector and circular profiles is taken as 90°. Their experimental database was formed from the results from 17 published studies covering both liquids and gases. Their method is applicable to the following range of parameters: $0.1 < e/d_i < 0.2$, $0.1 < p/d_i < 7.0$, $0.3 < \beta/90 < 1.0$, $5000 < Re < 250000$ and $0.66 < Pr < 37.6$.

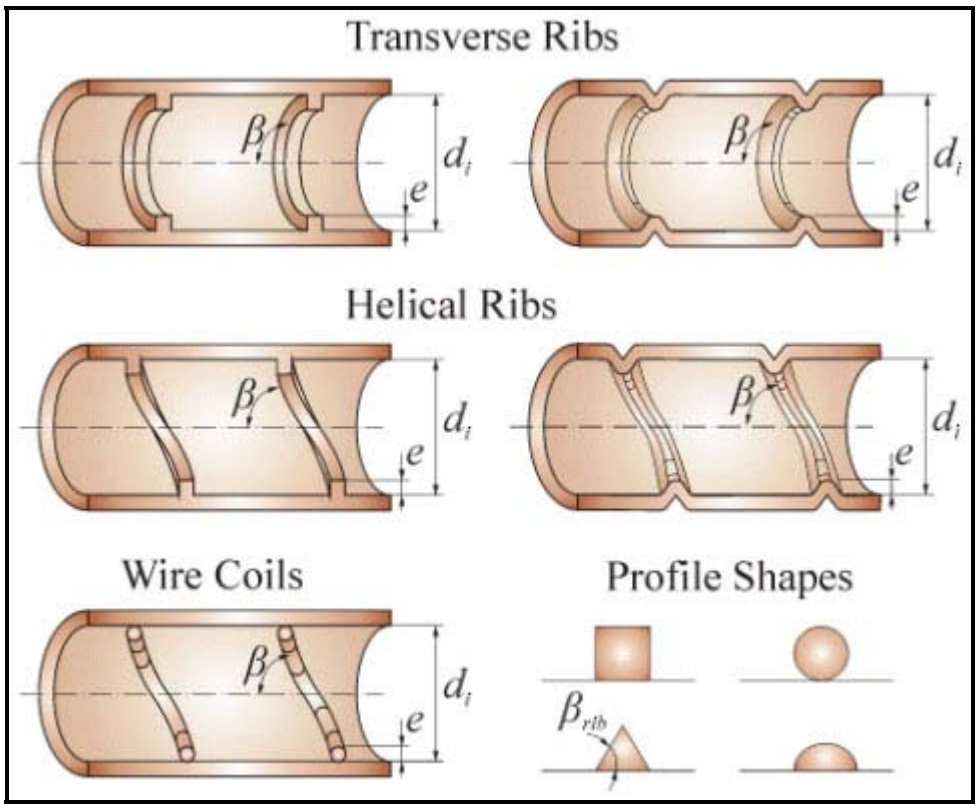

Figure 5.18. Internal enhancement geometries and profile shapes considered by Ravigururajan and Bergles (1985).

Their ribbed tube friction factor is correlated as a ratio to the value for a smooth tube of the same internal diameter as:

$$\frac{f_{ft}}{f} = \left\{1 + \left[29.1\,\mathrm{Re}^{(0.67 - 0.06\,p/d_i - 0.49\beta/90)} \left(\frac{e}{d_i}\right)^{(1.37 - 0.157\,p/d_i)} \right.\right.$$
$$\cdot \left(\frac{p}{d_i}\right)^{(-0.00000166\,\mathrm{Re} - 0.33\beta/90)} \left(\frac{\beta}{90}\right)^{(4.59 + 0.00000411\,\mathrm{Re} - 0.15\,p/d_i)} \qquad [5.6.8]$$
$$\left.\left. \cdot \left(1 + \frac{2.94}{n_{corners}}\right) \sin\beta_{rib} \right]^{15/16} \right\}^{16/15}$$

Equation [5.2.6] is used to determine the friction factor of the reference tube (smooth, plain internal surface tube) applying the wall-to-bulk property ratios as noted for that expression. The pressure drop is then obtained applying [5.2.7] using the ribbed tube friction factor in place of the plain tube value and using the diameter at the base of the ribs for d_i.

Their ribbed tube heat transfer correlation is

$$\frac{\alpha_{ft}}{\alpha_{pt}} = \left\{1 + \left[2.64\,\mathrm{Re}^{0.036} \left(\frac{e}{d_i}\right)^{0.212} \left(\frac{p}{d_i}\right)^{-0.21} \left(\frac{\beta}{90}\right)^{0.29} \mathrm{Pr}^{-0.024} \right]^7 \right\}^{1/7} \qquad [5.6.9]$$

Equation [5.2.8] is used to determine α_{pt} with [5.2.6] used to determine the friction factor of the reference tube (smooth, plain internal surface tube) applying the wall-to-bulk property ratios as noted for these expressions. Note that the heat transfer correlation does not contain any shape function and that the enhancement dimensions primarily control the level of augmentation while the flow parameters Re and Pr have small exponents and hence little influence.

Their friction factor correlation predicted 96% of their database to within ±50% and 77% to within ±20% while their heat transfer correlation predicted 99% of their database to within ±50% and 69% to within ±20%, for all five types of ribs and coiled wires they addressed. As a further note about this method, numerous comparisons to other independent or newer data and even to single-phase microfin data (*unpublished comparisons made by the present author*) show that these independent results are nearly always predicted to within ±20%, even when extrapolating the method to lower values of e/d_i, p/d_i and $\beta/90$. Thus, this method is both accurate and reliable. Furthermore, personal experience has shown that for trapezoidal profile ribs with rounded corners (typical of most commercially available ribbed tubes), the heat transfer correlation works well without modification while the friction factor is close to the mean of the values determined with $\beta_{ribs} = 2$ and $\beta_{ribs} =$ infinity.

Example 5.4: Heat transfer and pressure drop in a ribbed tube

For a liquid flowing inside a ribbed tube (e = 1.4 mm, β = 30° with 20 rectangular ribs), determine the local heat transfer coefficient and pressure drop at a mass velocity is 500 kg/m^{2}s assuming the internal diameter at the root of the ribs is 15.75 mm (0.620 in.) and the tube length is 3 m (9.84 ft). The physical properties of the fluid are: ρ = 997 kg/m^3; μ_{bulk} = 0.0007 Ns/m^2; μ_{wall} = 0.0005 Ns/m^2; k = 0.6 W/m K; c_p = 4200 J/kg K; Pr = $c_p\mu/k$ = 4.9.

***Solution*:** Applying [5.1.1] the axial pitch is found to be 4.285 mm. The Reynolds number Re is determined using [5.2.2] as:

$$\mathrm{Re} = \frac{\dot{m}\,d_i}{\mu_L} = \frac{500(0.01575)}{0.0007} = 11250$$

The plain and ribbed tube friction factors from [5.2.6] and [5.6.8] are:

$$f = \left(1.58\ln 11250 - 3.28\right)^{-2}\left(\frac{0.0007}{0.0005}\right)^{-0.25} = 0.00700$$

$$\frac{f_{ft}}{f} = \left\{1 + \left[29.1(11250)^{\left(0.67 - 0.06\left(\frac{0.004285}{0.01575}\right) - 0.49\left(\frac{30}{90}\right)\right)}\left(\frac{0.0014}{0.01575}\right)^{\left(1.37 - 0.157\left(\frac{0.004285}{0.01575}\right)\right)}\right.\right.$$

$$\left.\cdot\left(\frac{0.004285}{0.01575}\right)^{\left(-0.00000166(11250) - 0.33\left(\frac{30}{90}\right)\right)}\left(\frac{30}{90}\right)^{\left(4.59 + 0.00000411(11250) - 0.15\left(\frac{0.004285}{0.01575}\right)\right)}\right.$$

$$\left.\left.\cdot\left(1 + \frac{2.94}{2}\right)\sin 90\right]^{15/16}\right\}^{16/15}$$

$$f_{ft} = 1.233(0.00700) = 0.00863$$

The pressure drop in a tube of length L = 3.0 m is given by [5.2.7] to be:

$$\Delta p = \frac{2f\dot{m}^2 L}{\rho d_i} = \frac{2(0.00863)(500^2)(3.0)}{(997)(0.01575)} = 824\text{Pa}$$

Using [5.5.2] and [5.2.8] give:

$$\frac{\alpha_{ft}}{\alpha_{pt}} = \left\{1 + \left[2.64(11250)^{0.036}\left(\frac{0.0014}{0.01575}\right)^{0.212}\left(\frac{0.004285}{0.01575}\right)^{-0.21}\left(\frac{30}{90}\right)^{0.29}4.9^{-0.024}\right]^7\right\}^{1/7}$$

$$\alpha_{pt} = \left(\frac{0.6}{0.01575}\right)\frac{(0.007/2)(11250 - 1000)4.9}{1 + 12.7(0.007/2)^{1/2}\left(4.9^{2/3} - 1\right)}\left(\frac{0.0007}{0.0005}\right)^{0.14} = 2905\ \text{W/m}^2\text{K}$$

$$\alpha_{ft} = 2.036(2905)$$

$$\alpha_{ft} = 5915\ \text{W/m}^2\text{K}$$

Hence, for this internal rib design the heat transfer augmentation is 2.036 times the equivalent plain tube while its pressure drop is only 1.233 times larger.